RSC Advances

PAPER

View Article Online
View Journal | View Issue

Cite this: *RSC Adv.*, 2024, **14**, 28469

An AIE probe for the fluorescence and colorimetric sensing of La^{3+}†

Wan-Ying Lin,‡[de] Zi-Ao Zong,‡*[ac] Jing Wang,[c] Qi Huang,[f] Zhi-Yong Xing,[c] Chuan-Bin Fan[a] and Na-Na Li*[b]

Received 25th February 2024
Accepted 24th August 2024

DOI: 10.1039/d4ra01445f

rsc.li/rsc-advances

In this work, a fluorescent probe **N** with aggregation-induced emission effect was synthesized by grafting naphtho[2,3-*c*]furan-1,3-dione and 2-hydrazinylbenzo[*d*]thiazole. The probe **N** could recognize La^{3+} selectively and sensitively accompanied with an obvious fluorescence and color change from green to blue. Moreover, with the help of AIE properties, probe N achieved the detection of La^{3+} in the solid state.

1. Introduction

La^{3+}, a transition metal ion, is useful for radiotherapeutic applications, catalysis, and the synthesis of nanosized materials.[1–3] Additionally, La^{3+} binds strongly to the Ca^{2+} binding sites in proteins owing to their size equivalence.[4–6] Due to the increased utility of lanthanum compounds in the industry, their discharge into the environment poses a greater threat to life.[7–10] Therefore, the accurate determination of La^{3+} is of great significance for human health and environmental monitoring. In recent years, fluorescent probes have been developed as a useful tool for analyte detection because of their low cost, simple operation and potential applications in environmental and biological systems.[11–15] Thus, the development of fluorescent probes for sensing La^{3+} is necessary.

Huang's team synthesized a calix[6]arene-based fluorescent probe for fluorescence enhancement detection of La^{3+} ions in solution.[16] Areti *et al.* developed a glucopyranosyl conjugate as a fluorescent probe for the fluorescence turn on detection of La^{3+} in solution and living cells.[17]

Yang's team reported a coumarin-based fluorescent probe for the fluorescence turn-on detection of La^{3+} in solution and living cells.[18] However, these reported fluorescent probes displayed "turn on" response to La^{3+}, which is not obvious for La^{3+} detection by the naked eye. To date, AIE-active fluorescent probes have received considerable attention because they can emit strongly in the aggregated or solid state, detecting analytes in the aggregated states *via* a fluorescence colorimetric method.[19–25] Therefore, the development of AIE probes for La^{3+} is urgent.

In this work, we reported an AIE probe **N**, which displayed fluorescence colorimetric response towards La^{3+}. Additionally, the sensing mechanism of probe **N** for La^{3+} was proved using FT-IR, NMR and HRMS and further demonstrated through DFT calculations. Furthermore, probe **N** exhibited intense yellow–green emission in the solid state and could detect La^{3+} in the solid state, resulting in obvious fluorescence and color change. In addition, the comparison of the common methods and probe molecules of probe **N** with the previously reported La^{3+} probes is shown in Table S1.†

2. Experimental

2.1. General comments

^{1}H NMR spectra were recorded on a Bruker AV-600 spectrometer in d_6-DMSO. IR spectra were recorded with a PerkinElmer IR spectrophotometer. A Pgeneral TU-2550 UV-vis spectrophotometer and a PerkinElmer LS55 fluorescence spectrometer were employed to measure absorption and fluorescence spectra, respectively. Mass spectra were acquired on an Agilent 6220 Quadruple LC/MS (Agilent Co, USA). X-ray diffraction data were collected on a Bruker Smart CCD X-ray single-crystal diffractometer. TEM studies were carried out using a Maerwen zs90 scanning electron microscope at 100 kV. DLS data were obtained using a JEM-2100F nanometer laser particle analyzer.

All the materials for synthesis and spectral analysis are commercially available and used without further purification. The stock solutions (10 mM) of various metal ions were prepared from $AgNO_3$, KCl, $MgCl_2\cdot 6H_2O$, $Ba(ClO_4)_2$, $Zn(NO_3)_2\cdot 6H_2O$, $Cu(NO_3)_2\cdot 3H_2O$, $Cd(NO_3)_2\cdot 4H_2O$, $Pb(NO_3)CoSO_4\cdot 7H_2O$, $NiCl_2\cdot 6H_2O$, $CaCl_2$, $Al(NO_3)_3\cdot 9H_2O$, $MnCl_2\cdot 4H_2O$, $HgCl_2$,

[a]*Modern Industrial College of Biomedicine and Great Health, Youjiang Medical University for Nationalities, Baise, China. E-mail: zongziao@126.com*

[b]*Department of Chemistry, Xinzhou Normal University, Xinzhou, China. E-mail: LMT13643562571@126.com*

[c]*Key Laboratory of Research on Environment and Population Health in Aluminium Mining Areas (Youjiang Medical University for Nationalities), Education Department of Guangxi Zhuang Autonomous Region, Baise, China*

[d]*Affiliated Hospital of Youjiang Medical University for Nationalities, Baise, China*

[e]*Guangxi Key Laboratory for Biomedical Material Research, Baise, China*

[f]*Baise Center for Disease Control and Prevention, Baise, China*

† Electronic supplementary information (ESI) available. See DOI: https://doi.org/10.1039/d4ra01445f

‡ These authors contributed equally to this work.

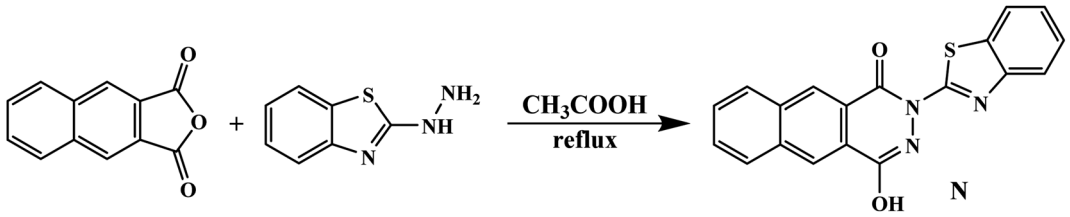

Scheme 1 Synthesis route of probe **N**.

Na_2SO_4, $FeCl_2 \cdot 4H_2O$, $FeCl_3 \cdot 6H_2O$, $LiNO_3$, $La(NO_3)_3 \cdot 6H_2O$, $SrCl_2 \cdot 6H_2O$, and $Bi(NO_3)_3 \cdot 5H_2O$. The pH of **L** solution was adjusted with HCl and NaOH aqueous solutions. For fluorescence measurements, the excitation wavelength was 380 nm and the excitation and emission wavelength band passes were both set at 5 nm.

2.2. Synthesis

As shown in Scheme 1, naphtho[2,3-*c*]furan-1,3-dione (198 mg, 1 mmol) and 2-hydrazinylbenzo[*d*]thiazole (165 mg, 1 mmol) were dissolved in 10 mL glacial acetic acid solution and stirred for 5 h.[26] After the completion of the reaction, the solvent was cooled to room temperature and filtered to obtain a pale green compound (169 mg, yield 49%). ^{1}H NMR (Fig. S1†) (600 MHz, DMSO) δ 11.07 (s, 1H), 8.63 (s, 2H), 8.29 (t, 2H), 7.82 (m, 3H), 7.43 (m, 1H), 7.30 (m, 1H), 7.16 (m, 1H). ^{13}C NMR (Fig. S2†) (151 MHz, DMSO-d6) δ (ppm) 191.21, 179.17, 171.63, 162.30, 160.82, 133.05, 131.69, 130.72, 130.25, 127.87, 127.39, 126.69, 124.64, 124.11, 116.54, 112.49, 106.47, 60.97, 55.87. ESI-MS (Fig. S3†): calcd for $C_{22}H_{26}N_3OS$: 346.06502 [**N** + H]$^+$, found: 346.06381.

3. Results and discussion

3.1. The optical properties of AIE

As shown in Fig. 1a, probe **N** displayed obvious green fluorescence with emission peaks at 515 nm and 467 nm. The fluorescence spectra of probe **N** (10^{-5} M) in EtOH/H_2O mixture with different water fractions (f_w) were illustrated in Fig. 1b for studying the AIE properties. The probe **N** in pure ethanol solution displayed a maximum emission near 475 nm and blue fluorescence was observed. The fluorescence intensity at 475 nm starts to decrease after water fraction higher than 10% and a new shoulder peak appeared at 545 nm. When $f_w = 90\%$, the emission peak at 545 nm reached the maximum. In addition, probe **N** showed average particle diameter with 255 nm in EtOH and 295 nm in 90% water, respectively (Fig. S4†). The result suggested that water molecule induced the aggregation of probe **N** molecules. The above results indicated that the probe **N** possessed AIE activity.

3.2. Fluorescence spectra studies of probe N

The sensing ability of probe **N** towards various analytes (Ag^+, K^+, Na^+, Li^+, Pb^{2+}, Mg^{2+}, Ca^{2+}, Zn^{2+}, Cd^{2+}, Mn^{2+}, Ba^{2+}, Hg^{2+}, Co^{2+}, Ni^{2+}, Sr^{2+}, Al^{3+}, Fe^{3+}, Cr^{3+}, Bi^{3+}, La^{3+} and Cu^{2+}) was examined in the EtOH–H_2O (v/v = 1/9, pH 7.4) system (Fig. 2a). The emission peak at 545 nm of probe **N** was blue-shifted to the 460 nm along with obvious fluorescence enhancement and the fluorescence and color changed from green to blue under 365 nm UV lamp after the addition of the La^{3+} ion. However, upon the addition of the above other metal ions, the fluorescence intensity of probe **N** displayed insignificant changes. Therefore, the selectivity of probe **N** towards La^{3+} was supported by fluorescence spectra or naked eyes.

The competition experiments were carried out in the presence of the above metal ions by measuring the fluorescence intensity at 475 nm under the same condition (Fig. S5†). The

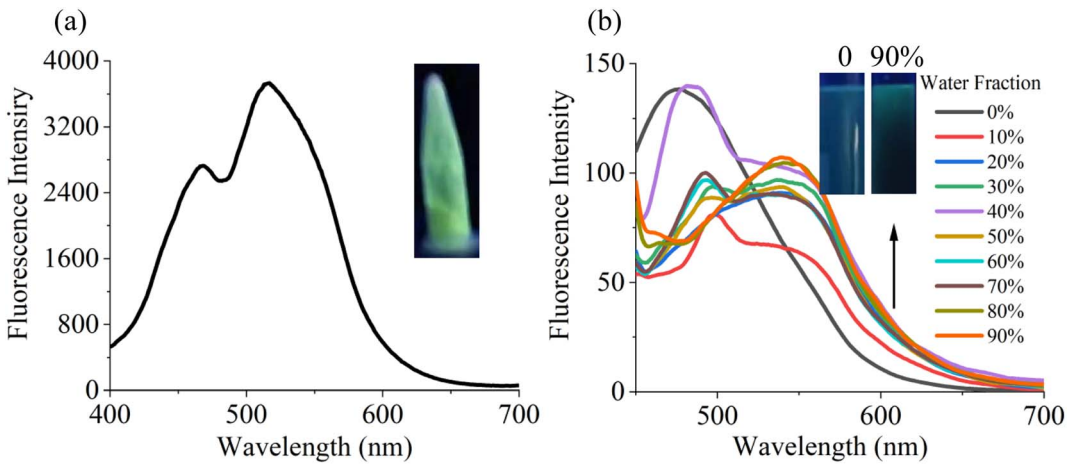

Fig. 1 (a) The emission spectra of probe **N** in the solid state. (b) Fluorescence spectra of probe **N** (10 μM) in EtOH/H_2O with different water fractions.

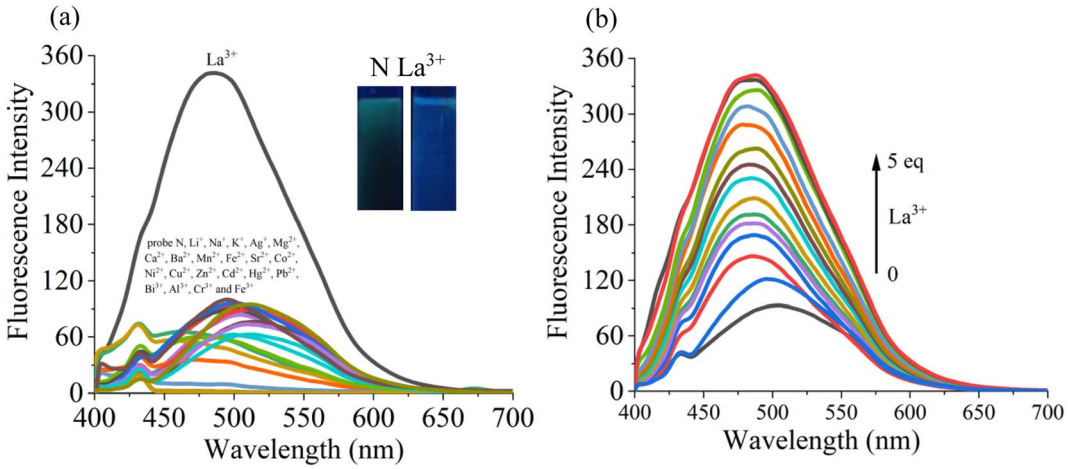

Fig. 2 (a) Fluorescence spectra of probe **N** (10 μM) in the presence of various metal ions (50 μM) in EtOH/H_2O (9/1, v/v, pH = 7.4) medium. Inset: The color change of probe **N** (10 μM) before and after the addition of La^{3+} (50 μM) in the EtOH/H_2O (1/9, v/v, pH = 7.4) medium under 365 nm UV light. (b) The fluorescence spectra of probe **N** (10 μM) upon the addition of different concentrations of La^{3+} in the EtOH/H_2O (1/9, v/v, pH = 7.4) medium.

probe **N** (10 μM) was treated with La^{3+} (50 μM) in the presence of the above metal ions (50 μM) with the same concentration, respectively. **N**–La^{3+} still displayed the obvious emission in the presence of other metal ions except for Co^{2+} and Cu^{2+}, indicating that probe **N** showed high sensitivity to La^{3+}.

In addition, the fluorescence titrations for La^{3+} were carried out in EtOH–H_2O (v/v = 1/9, pH 7.4) solution. In Fig. 2b, as the concentration of La^{3+} increased from 10 μM to 10 μM, the fluorescence intensity exhibited a gradual increase and the maximum emission wavelength was blue shifted to 475 nm. Also, the good linear fit range of probe **N** to La^{3+} (0–30 μM) was observed. The limit of detection (LOD) of probe **N** to La^{3+} was calculated to be 3.6×10^{-7} M based on the $3\sigma/k$ criterion (where σ is the standard deviation of the blank measurements, and k is the slope of the intensity ratio *versus* sample concentration plot). Therefore, the above results indicated that probe **N** could quantitatively detect La^{3+}.

3.3. Sensing mechanism of probe N for La^{3+}

To explore the sensing mechanism of probe **N** with La^{3+}, the ^1H NMR (Fig. S6†), FT-IR (Fig. S7†) and HRMS spectra (Fig. S8†) of probe **N** and **N** + La^{3+} were measured. In the ^1H NMR spectra (Fig. S4†), after the addition of 1 equiv. La^{3+}, the OH proton (Ha) at 11.1 ppm disappeared, indicating the occurrence of the deprotonation process in the presence of La^{3+} (Scheme 2). Also, the characteristic –OH absorption peak at 3450 cm^{-1} and the characteristic –C=N absorption peak at 1658 cm^{-1} disappeared, indicating that the N atom in the –C=N group and the O atom in the –C=N group might interact with La^{3+}. Further, the HRMS of **N** + La^{3+} were measured in the EtOH/H_2O (1/9, V/V, pH = 7.4) solution. We found m/z = 544.93903, which could be assigned to [**N** − H + La^{3+} + NO_3^-]$^+$ (m/z, Cal, 544.94354), suggesting that a certain complex was formed between probe **N** and La^{3+}. Therefore, according to the above analysis, a possible sensing mechanism of probe **N** for La^{3+} is proposed in Scheme 2. The stoichiometry of probe **N** with La^{3+} was further confirmed by Job's plot analysis (Fig. S7†). The total concentration of probe **N** and La^{3+} was kept constant at 10 μM during this experimental process, and the variable molar fraction of La^{3+} was varied from 0.1 to 0.9. In the Job's plot (Fig. S9†), the fluorescence intensity at 486 nm for **N** + La^{3+} showed peaks when the molecular fraction of La^{3+} was close to 0.5, further suggesting the 1 : 1 binding stoichiometry between probe **N** and La^{3+}. Based on the above results, the possible sensing mechanisms of probe **N** with La^{3+} are proposed in Scheme 2.

In addition, density functional theory (DFT) calculation was performed to further understand the sensing mechanism of probe **N** to La^{3+}. First, the structures of probe **N** and **N** + La^{3+} were optimized, and the highest occupied molecular orbital (HOMO) and the lowest unoccupied molecular orbital (LUMO) are shown in Fig. 3. For probe **N**, the electron cloud distribution in the LUMO (−2.08 eV) was mainly from the naphthalene ring, while the electron cloud distribution in the HOMO (−6.22 eV)

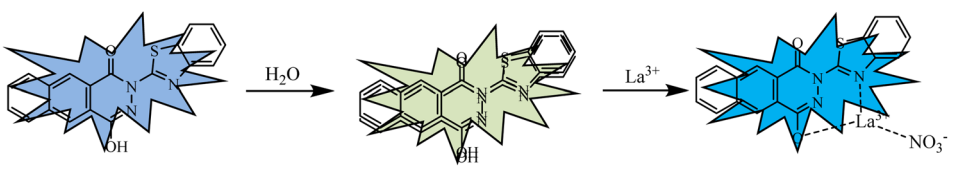

Scheme 2 Plausible sensing mechanism of probe **N** for La^{3+}.

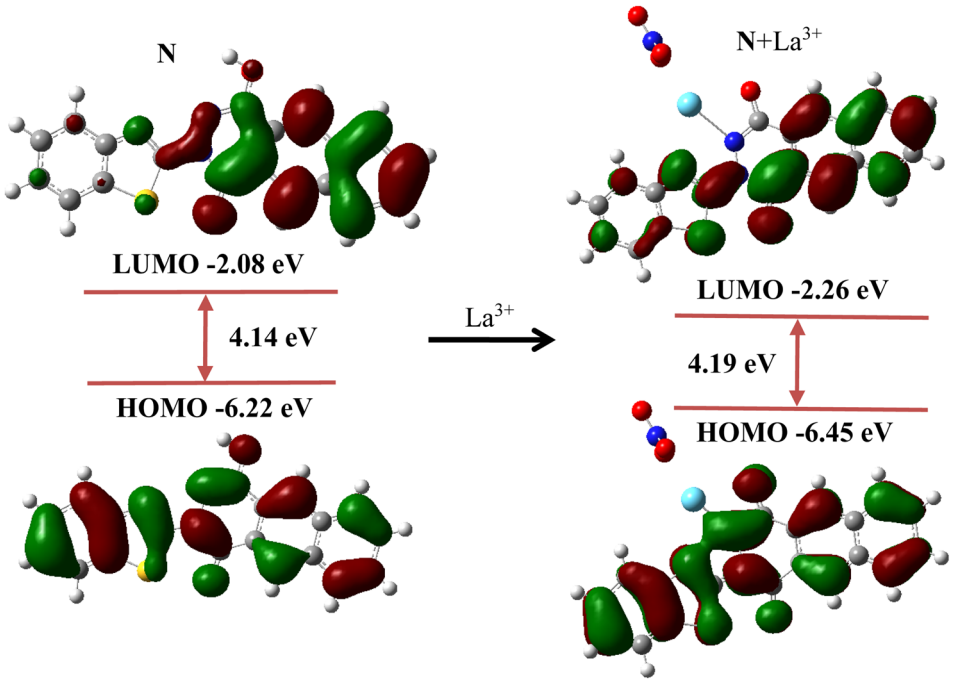

Fig. 3 The calculated molecular orbitals and the HOMO–LUMO gaps of probe **N** and **N** + La^{3+}.

was determined by the entire molecular skeleton. For **N** + La^{3+}, the electron cloud distribution in the LUMO was spread on the partial molecular skeleton, while the electron cloud distribution in the HOMO was mainly localized over the whole conjugated skeleton. The HOMO–LUMO energy gap for probe **N** and **N** + La^{3+} was found to be 4.14 eV and 4.19 eV, respectively.

3.4. Application in the solid state

We investigated the solid-state sensing behaviour because of the AIE effect of probe **N**. We added La^{3+} to probe **N**, gently mixed it and recorded the fluorescence spectrum (Fig. 4). After the interaction of probe **N** with La^{3+}, the emission peak from 530 nm blue shifted to 476 nm, and the obvious fluorescence change from yellow–green to blue emission was observed. These results indicated that probe **N** could be used to colorimetrically detect La^{3+} by naked eye in the solid state.

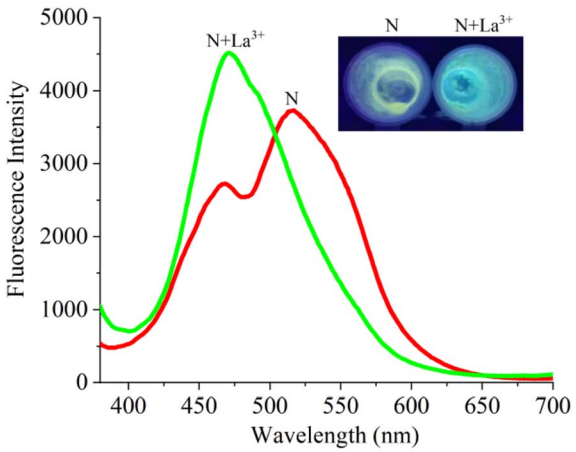

Fig. 4 Fluorescence spectral changes of probe **N** in the absence and presence of La^{3+} in the solid state. Inset: the color change in probe **N** in the absence and presence of La^{3+} in the solid state under 365 nm UV light.

4. Conclusion

In conclusion, we developed a fluorescent probe **N** using a one-step reaction and it displayed AIE characteristics. Probe **N** could serve as a fluorescence colorimetric probe for La^{3+}. Furthermore, probe **N** exhibited fluorescence and color change from yellow to green for La^{3+} in the solid state.

Data availability

The authors confirm that the data supporting the findings of this study are available within the article and its ESI.†

Author contributions

Conceptualization, Z. A. Z.; methodology, Z. A. Z. and W. Y. L.; formal analysis, C. B. F.; data curation, Q. H. and J. W.; writing—original draft preparation, Z. Y. X. and N. N. Li.; writing—review and editing, C. B. F. and N. N. Li.

Conflicts of interest

The authors declare no conflict of interest.

Acknowledgements

This work was supported by Scientific and Technological Innovation Programs of Higher Education Institutions in Shanxi (No. 2022L465), Fundamental Research Program of Shanxi Province (No. 202203021222307), Xinzhou Teachers University project fund (No. 00001036), the Scientific Research and Technology Development Program Project of Baise City (No. 20222001), the Science and Technology Baseand the Talent Special Project for Guangxi Province (No. AD22035154 and AD20297056).

References

1 F. Albaaj and A. J. Hutchison, Lanthanum carbonate for the treatment of hyperphosphataemia in renal failure and dialysis patients, *Expert Opin. Pharmacother.*, 2005, **6**, 319–328.

2 T. Vairapperumal, D. Natarajan, K. M. Syamala, S. K. Janardhanan and N. B. Unni, Catechin caged lanthanum orthovanadate nanorods for nuclear targeting and bioimaging applications, *Sens. Actuators, B*, 2017, **242**, 700–709.

3 L. Feng, H. Xiao, X. He, Z. Li, F. Li, N. Liu, Z. Chai, Y. Zhao and Z. Zhang, Long-term effects of lanthanum intake on the neurobehavioral development of the rat, *Neurotoxicol. Teratol.*, 2006, **28**, 119–124.

4 A. Benedetto, C. Bocca, P. Brizio, S. Cannito, M. C. Abete and S. Squadrone, Effects of the rare elements lanthanum and cerium on the growth of colorectal and hepatic cancer cell lines, *Toxicol. In Vitro*, 2018, **46**, 9–18.

5 T. M. Palanivel, N. Sivakumar, A. Al-Ansair and R. Victor, Bioremediation of copper by active cells of Pseudomonas stutzeri LA3 isolated from an abandoned copper mine soil, *J. Environ. Manage.*, 2020, **253**, 109706.

6 L. Yang, T. Liu, Z. Li, F. Wang and C. Wu, Adsorption of La^{3+} onto trifluoroacetic acid modified UiO-66-COOH: Adsorption mechanism and application, *Mater. Chem. Phys.*, 2023, **301**, 127535.

7 C. Liu, T. Qiu, L. Feng and Y. Chen, Synthesis of temperature-sensitive ion-imprinted polymer based on chitosan for selective separation of La^{3+} from aqueous solution: Effect of different salt anions in the template, *J. Environ. Chem. Eng.*, 2020, **253**, 109706.

8 J. Hu, K. Wan, X. Deng, X. Liu, Y. Fang, F. Zhou, J. Yu, R. Chi and C. Xiao, Metagenomic analysis revealed the evolution of microbial communities, metabolic pathways, and functional genes in the heterotrophic nitrification-aerobic denitrification process under La^{3+} stress, *Sci. Total Environ.*, 2024, **912**, 169243.

9 Y. Chen, Y. Shen, Y. Zhao, J. Zhu and H. Wang, Rapid detection of zearalenone in cereals using La^{3+}-doped upconversion nanoparticles-based immunochromatographic assay, *Food Control*, 2023, **153**, 109904.

10 Q. Y. Liu, Y. F. Yu, C. J. Liu, Y. H. Liu, L. J. Yuan, Z. Wang and A. X. Yu, Effect of La^{3+} and Mg^{2+} combined system on bioactivity and osteogenesis of bioinspired La-doped magnesium phosphate composites prepared utilizing the precursor method, *J. Mater. Res. Technol.*, 2023, **24**, 9523–9536.

11 J. T. Hou, K. Kwon, S. Wang, B. Y. Wang, X. J. He, J. Yoon and J. L. Shen, Sulfur-based fluorescent probes for HOCl: Mechanisms, design, and applications, *Coord. Chem. Rev.*, 2022, **450**, 214232.

12 Y. Feng, S. S. Hu, Y. Z. Wang, X. R. Song, C. Cao, K. Wang, C. L. Jing, G. L. Zhang and W. S. Liu, A multifunctional fluorescent probe for visualizing H_2S in wastewater with portable smartphone via fluorescent paper strip and sensing GSH in vivo, *J. Hazard. Mater.*, 2021, **406**, 124523.

13 Y. T. Yang, T. T. Zhou, M. Jin, K. Y. Zhou, D. D. Liu, X. Li, F. J. Huo, W. Li and C. X. Yin, A thiol-chromene "click" reaction triggered self-immolative for NIR visualization of thiol flux in physiology and pathology of living cells and mice, *J. Am. Chem. Soc.*, 2020, **142**(3), 1614–1620.

14 T. T. Yu, P. Sun, Y. J. Hu, Y. G. Ji, H. P. Zhou, B. W. Zhang, Y. P. Tian and J. Y. Wu, A novel and simple fluorescence probe for detecting main group magnesium ion in Hela cells and Arabidopsis, *Biosens. Bioelectron.*, 2016, **86**, 677–682.

15 S. Das, A. Sarkar, A. Rakshit and A. Datta, A Sensitive Water-Soluble Reversible Optical Probe for Hg^{2+} Detection, *Inorg. Chem.*, 2018, **57**, 5273–5281.

16 J. M. Liu, C. F. Chen, Q. Y. Zheng and Z. T. Huang, A selective fluorescent probe for La^{3+} and Y^{3+} based on calix[6]arene, *Tetrahedron Lett.*, 2004, **45**, 6071–6074.

17 S. Areti, S. Bandaru, R. Teotia and C. P. Rao, Water-Soluble 8-Hydroxyquinoline Conjugate of Amino-Glucose As Receptor for La^{3+} in HEPES Buffer, on Whatman Cellulose Paper and in Living Cells, *Anal. Chem.*, 2015, **87**, 12348–12354.

18 G. Zhou, X. Wang and Y. Yang, A new coumarin derivative as a highly selective "turn-on" fluorescence probe for La^{3+} (lanthanum ion) in living zebrafis, *J. Photochem. Photobiol., A*, 2024, **447**, 115264.

19 Y. Hong, J. W. Y. Lam and B. Z. Tang, Aggregation-induced emission, *Chem. Soc. Rev.*, 2011, **40**, 5361–5388.

20 B. Guo, W. Shu, W. Liu, H. Wang, S. Xing, J. Chen and X. Zhang, Mitochondria-specific ultrasensitive ratiometric AIE probe for imaging endogenous peroxynitrite, *Sens. Actuators, B*, 2021, **344**, 130206.

21 X. Kong, M. Li, Y. Zhang, Y. Yin and W. Lin, Engineering an AIE N_2H_4 fluorescent probe based on α-cyanostilbene derivative with large Stokes shift and its versatile applications in solution, solid-state and biological systems, *Sens. Actuators, B*, 2021, **329**, 129232.

22 Z. Y. Xu, L. Han, X. H. Wang, J. R. Chen, N. B. Li and H. Q. Luo, Rational construction of long-wavelength emissive AIE molecules and their application for sensitive and visual detection of HClO, *Sens. Actuators, B*, 2022, **352**, 131024.

23 X. M. Han, Y. F. Ma, Y. Z. Chen, X. F. Wang and Z. Wang, Enhancement of the Aggregation-Induced Emission by Hydrogen Bond for Visualizing Hypochlorous Acid in an

Inflammation Model and a Hepatocellular Carcinoma Model, *Anal. Chem.*, 2020, **92**, 2830–2838.

24 H. F. Xie, X. H. Jiang, F. Zeng, C. M. Yu and S. Z. Wu, A novel ratiometric fluorescent probe through aggregation-induced emission and analyte-induced excimer dissociation, *Sens. Actuators, B*, 2014, **203**, 504–510.

25 A. B. Zhang, L. Jin, Q. M. Wang, W. L. Wang and Y. L. Chen, Two smart coumarin-based fluorescent probes with AIE effect for sensing ClO^- and imaging in living cells, *Spectrochim. Acta, Part A*, 2022, **283**, 121690.

26 N. N. Li, N. N. Shi, D. Yang, R. X. Wu, C. G. Xu, B. Zhu, X. Shao, X. Zhang, S. Y. Bi and Y. H. Fan, Solid-state fluorescent switch based on the intercoversion of J-aggregation and dimer and aggregation pattern-dependent fluorescence colorimetric sensing of GSH/Zn^{2+}/Cd^{2+}, *J. Mol. Liq.*, 2021, **342**, 116946.